Spin chirality on a two-dimensional frustrated lattice

DANIEL GROHOL[1], KITTIWIT MATAN[2], JIN-HYUNG CHO[2], SEUNG-HUN LEE[3], JEFFREY W. LYNN[3], DANIEL G. NOCERA[1] AND YOUNG S. LEE[2]*

[1]Department of Chemistry, Massachusetts Institute of Technology, Cambridge, Massachusetts 02139, USA
[2]Department of Physics and Center for Materials Science and Engineering, Massachusetts Institute of Technology, Cambridge, Massachusetts 02139, USA
[3]NIST Center for Neutron Research, Gaithersburg, Maryland 20899, USA
*e-mail: younglee@mit.edu

Published online: 27 March 2005; doi:10.1038/nmat1353

The collective behaviour of interacting magnetic moments can be strongly influenced by the topology of the underlying lattice. In geometrically frustrated spin systems, interesting chiral correlations may develop that are related to the spin arrangement on triangular plaquettes. We report a study of the spin chirality on a two-dimensional geometrically frustrated lattice. Our new chemical synthesis methods allow us to produce large single-crystal samples of $KFe_3(OH)_6(SO_4)_2$, an ideal Kagomé lattice antiferromagnet. Combined thermodynamic and neutron scattering measurements reveal that the phase transition to the ordered ground-state is unusual. At low temperatures, application of a magnetic field induces a transition between states with different non-trivial spin-textures.

Geometrically frustrated magnets are unusual in that they may have disordered ground states in which an enormous number of spin configurations share the same energy[1,2]. The Kagomé lattice antiferromagnet, formed of corner-sharing triangles, is one of the most highly frustrated two-dimensional (2D) lattices. Although long regarded as a prime model for studying spin frustration[1,3–6], the Kagomé lattice has escaped precise magnetic characterization because compounds that form this lattice are difficult to make pure and in large single-crystal form. We present a study of an ideal Kagomé lattice compound, the iron jarosite $KFe_3(OH)_6(SO_4)_2$. This material possesses robust chiral correlations related to the arrangement of spins around triangular plaquettes[7,8]. The presence of spin chirality in condensed-matter systems may play a role in important phenomena ranging from high-temperature (high-T_C) superconductivity[9] to the anomalous Hall effect[10,11]. Currently, there are few experimental studies of spin chirality in frustrated magnets. Here, we study the non-trivial spin-textures related to chirality in a jarosite material in both the spin-ordered and spin-disordered states. Our measurements of magnetic susceptibility, specific heat and magnetic neutron scattering on pure single crystals show that the transition to the low-temperature ordered phase is unusual. In addition, we find that the spin texture of the ground state can be controlled by applying a magnetic field.

The magnetic Fe^{3+} ions of jarosite have spin-5/2 and lie at the corners of the triangles of the Kagomé lattice, shown in Fig. 1. To first approximation, the spin hamiltonian is given by:

$$H = \sum_{<i,j>} J\,\mathbf{S}_i \cdot \mathbf{S}_j$$

where J is the nearest-neighbour magnetic exchange interaction ($J > 0$). Because the interaction is antiferromagnetic, the spin system is frustrated, and the corner-sharing arrangement leads to a higher degree of degeneracy for the ground state than for the triangular lattice. The iron jarosite is a particularly ideal Kagomé lattice compound for the following reasons. First, it consists of single layers of undistorted Kagomé planes, and these planes remain undistorted

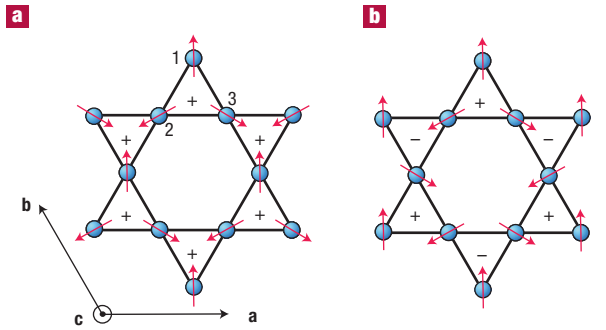

Figure 1 The Kagomé lattice with spins arranged in two different configurations. a, The '$q = 0$' structure, which is the ground-state configuration for iron jarosite. The spin arrangement has uniform, positive vector chirality, indicated by the + within each triangular plaquette. **b**, An alternative spin arrangement with staggered vector chirality, known as the $\sqrt{3} \times \sqrt{3}$ structure.

down to the base temperatures of our measurements ($T \approx 5$ K). Second, this jarosite can be synthesized with compositions that are stoichiometrically pure, as we describe below. This ensures that we are primarily studying the effects of geometric frustration rather than the effects of disorder. Third, large single crystals can be made, which allow investigations of the spin correlations of this Kagomé compound that would not be possible with powder samples alone.

Until recently, jarosites have been prepared typically by precipitation under hydrothermal conditions:

$$3Fe^{3+} + 2K_2SO_4 + 6H_2O \rightarrow KFe_3(OH)_6(SO_4)_2 + 3K^+ + 6H^+ \quad (1)$$

Under these conditions, the monovalent K^+ cation is susceptible to replacement by hydronium ions and the coverage of the Fe^{3+} lattice sites is incomplete. Also, only microcrystalline materials are obtained owing to the heightened acidity of the solution as well as the speed and intractability of the precipitation reaction[7,12]. The challenges confronting the synthesis of pure jarosites have been overcome with the development of redox-based hydrothermal methods[13]. Control over the precipitation of the jarosite is achieved by inserting two oxidation–reduction steps before reaction (1):

$$Fe + 2H^+ \rightarrow Fe^{2+} + H_2 \quad (2)$$

$$2Fe^{2+} + \tfrac{1}{2}O_2 + 2H^+ \rightarrow 2Fe^{3+} + H_2O \quad (3)$$

In this manner, the Fe^{3+} is slowly generated throughout the course of the hydrothermal process and the pH is moderated because three overall equivalents of protons are consumed in the production of an equivalent of jarosite. We have refined the synthesis process to optimize the size of the single crystals. Crystals as large as 10 mm in length and 48 mg in mass have been grown, making possible the inelastic neutron scattering measurements that we discuss below. Details of the single-crystal synthesis may be found in the Supplementary Information.

Even though the Kagomé lattice antiferromagnet should not order at any non-zero temperature, powder neutron diffraction measurements on $KFe_3(OH)_6(SO_4)_2$ indicate that the spins order in a coplanar '$q = 0$' arrangement below the Néel temperature $T_N \approx 65$ K (refs 7,8). In the $q = 0$ structure, the spins on each triangle are oriented at 120° to each other, and the 2D magnetic unit cell is identical to the 2D structure unit cell, as shown in Fig. 1a. The ordered spins can be decomposed into

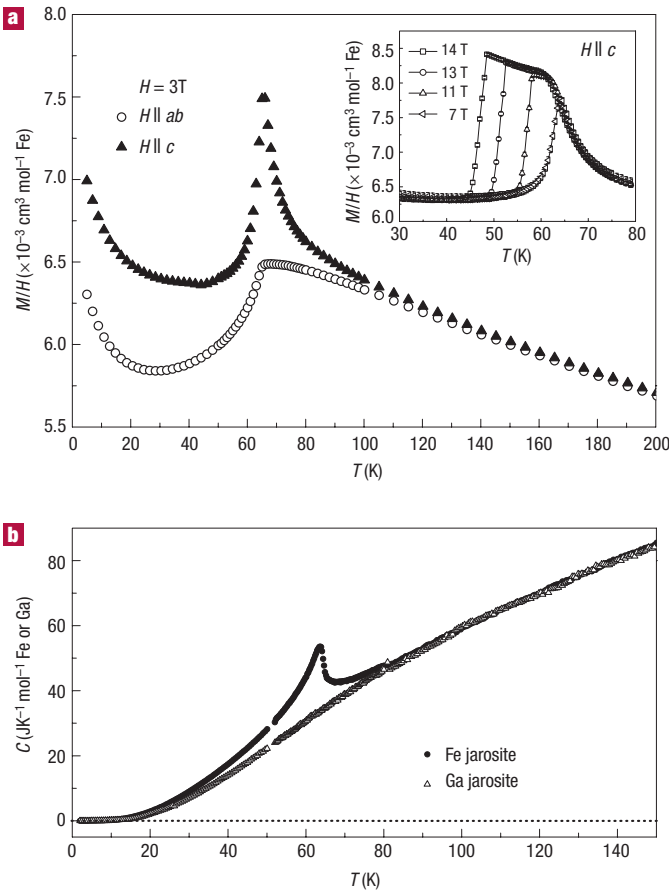

Figure 2 Magnetization and specific heat measurements of $KFe_3(OH)_6(SO_4)_2$. a, M/H versus temperature with the applied field in two orientations, $H \parallel c$ and $H \parallel ab$, measured on a single-crystal sample using a SQUID magnetometer. The inset shows M/H for $H \parallel c$ for fields up to 14 T measured using an a.c. coil set. The upturn in the magnetization at low temperatures (below 20 K) can be described by Curie behaviour in which the density of free spins corresponds to ~0.3% of the total number of spins. **b**, Specific heat of powder samples of $KFe_3(OH)_6(SO_4)_2$ (closed symbols) and the non-magnetic isostructural compound $KGa_3(OH)_6(SO_4)_2$ (open symbols). The $KGa_3(OH)_6(SO_4)_2$ data are scaled to match the Fe jarosite data at high temperatures and are used to estimate the phonon contribution.

three sublattices, with the spins on each triangle labelled as $\mathbf{S}_1$, $\mathbf{S}_2$ and $\mathbf{S}_3$. The vector chirality for each triangle may be defined as:

$$\mathbf{K}_V = [2/(3\sqrt{3})](\hat{\mathbf{S}}_1 \times \hat{\mathbf{S}}_2 + \hat{\mathbf{S}}_2 \times \hat{\mathbf{S}}_3 + \hat{\mathbf{S}}_3 \times \hat{\mathbf{S}}_1) \quad (4)$$

For the coplanar arrangement, this vector is parallel to the c axis with amplitude +1 or –1 (ref. 7). The neutron powder results[7,8] indicate that each triangle has positive chirality (+1) in the ordered state, such that the spins point directly towards or away from the centre of each triangle.

For this compound, as for all real magnetic materials, the interaction hamiltonian of the spins contains terms beyond isotropic Heisenberg exchange. These additional terms cause the system to order at a non-zero T_N and determine the ground-state spin arrangement. Currently, it is not clear whether the transition to long-range order is driven by weak interplanar coupling, spin anisotropy, anisotropic exchange or some combination of these. An ordered phase on a Kagomé lattice is characterized by two order parameters (the sublattice magnetization

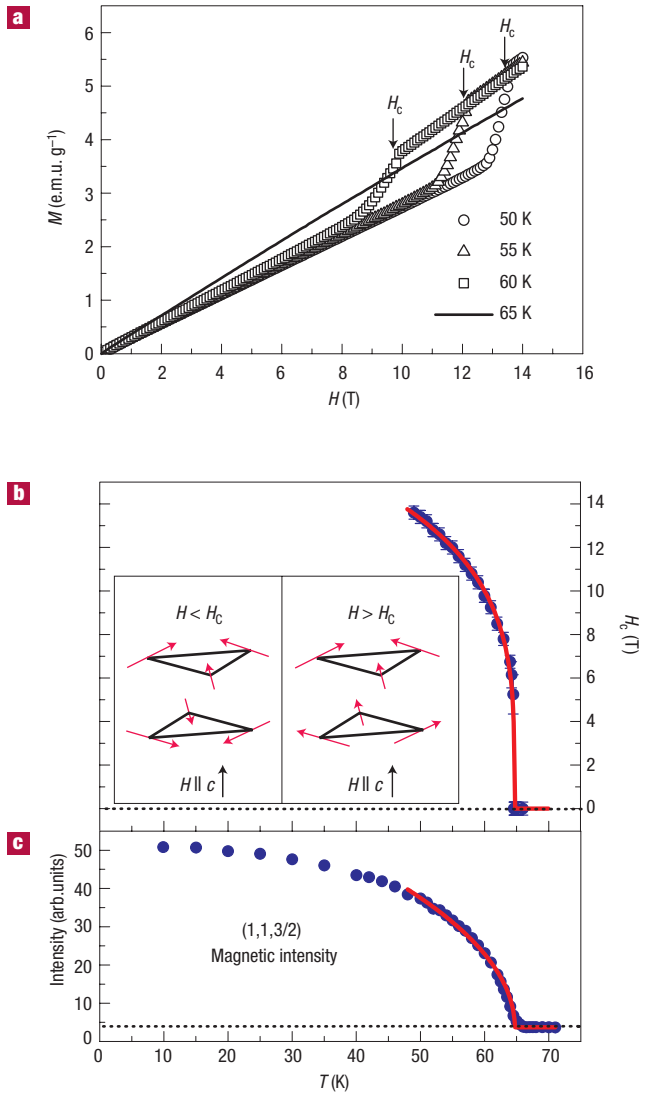

Figure 3 Measurements of the field-induced transition to a state with non-zero scalar chirality. a, Magnetization versus applied field for several temperatures with $H \parallel c$. The H_c values indicate the fields where dM/dH is maximum. **b**, Values of H_c versus temperature. The inset depicts the change in the spin configuration below and above H_c. **c**, Integrated intensity of the (1,1,3/2) magnetic Bragg peak measured with neutron diffraction on a single crystal in zero field. This quantity is proportional to $(M^{\dagger})^2$, the square of the staggered moment. The lines in **b** and **c** correspond to power-law forms for H_c and $M^{\dagger}$ with the exponent $\beta = 0.25$ and $T_N = 64.7$ K.

and the vector chirality), which have different symmetries. An intriguing possibility is that these symmetries are broken at different temperatures. This has been proposed as a result of numerical work on *XY* or planar triangular lattice systems[14,15]. However, it has not been conclusively observed by experiment[16,17]. For Kagomé lattice systems, relatively little is known about the nature of the phase transitions that occur.

MAGNETIZATION AND FIELD-INDUCED TRANSITION

To address the above issues, we have first measured the magnetization of a single crystal sample (mass of 13.5 mg) of $KFe_3(OH)_6(SO_4)_2$ using a SQUID magnetometer. Measurements were taken with the applied field oriented along the *c*-axis ($H \parallel c$), or within the *a*–*b* plane ($H \parallel ab$), as shown in Fig. 2a. At low fields ($H < 5$ T) with the field along *c*, a sharp peak appears near 65 K, indicative of the transition to the 3D magnetically ordered state. This is consistent with previous measurements on powder samples prepared under similar synthesis conditions[18]. When the field is aligned within the *a*–*b* plane, the sharp peak is absent and is replaced by a broad cusp.

In Fig. 2b, we plot the specific heat C of powder samples of $KFe_3(OH)_6(SO_4)_2$. A peak in the specific heat is found at the magnetic transition temperature of 65 K. The entropy associated with the 3D magnetic transition (integrating C/T over the temperature range from 2 K to 100 K) represents ~50% of the $R\ln 6$ (where R is the molar gas constant) total entropy expected for the spin-5/2 system. This suggests that short-range correlations have already formed at much higher temperatures.

At high temperatures ($T > 150$ K), the susceptibility is isotropic and follows a Curie–Weiss law $\chi = C/(T - \Theta_{CW})$, consistent with previous results on powder samples[18]. Fits to this law between 150 K and 550 K yield the values $\Theta_{CW} = -800(30)$ K, and $C = 5.6(2)$ cm^3 K (mol^{-1} Fe). Because the data are taken for $T < |\Theta_{CW}|$, we extract the effective moment μ_{eff} and the nearest-neighbour exchange coupling J using the high-temperature series analysis of Harris *et al.* for the Kagomé lattice[3]. Our results indicate that $J = 45(2)$ K $= 3.9(2)$ meV and $\mu_{eff} = 6.3(2)\mu_B$ (close to the spin-only value of $5.92\mu_B$ for Fe^{3+}). We note that a small next-nearest neighbour interaction ($J_2 > 0$) would serve to reduce the calculated value of J by an amount of order J_2.

The peak in M/H for $H \parallel c$ at $T = 65$ K indicates the presence of weak ferromagnetism along the *c* direction. Recent theoretical work[19] shows that antisymmetric exchange, by the Dzyaloshinsky–Moriya (DM) interaction, may induce such a moment by canting the spins slightly out of the plane. This interaction is present if there is no inversion centre between magnetic ions and adds the term:

$$\sum_{<i,j>} \mathbf{D} \cdot \left(\mathbf{S}_i \times \mathbf{S}_j \right)$$

to the spin hamiltonian, where **D** is the DM vector[20]. This interaction causes the spins on each triangle in the jarosite to form an 'umbrella' structure and gives each Kagomé plane a net ferromagnetic moment. However, the interlayer coupling in iron jarosite causes the ferromagnetic moments to couple antiferromagnetically between layers in the absence of an applied field, as shown in the inset of Fig. 3b. Our measurements on single crystals allow us to explore this model of canted moments. The inset of Fig. 2a shows M/H as a function of temperature measured in high fields ($H \geq 7$ T). At these high fields, the peak broadens and the downturn in the magnetization shifts to lower temperatures. Such behaviour has been observed[21] in the square-lattice antiferromagnet La_2CuO_4 for which the DM interaction does indeed result in weak ferromagnetism[22].

To investigate this spin canting further, we made magnetization measurements as a function of magnetic field along the *c* direction as shown in Fig. 3a. The results show an abrupt change in the magnetization at a critical field, H_C, which we define as the field at which dM/dH is a maximum. We interpret this abrupt increase as a change from canted moments being oppositely directed between planes to canted moments aligned in the same direction. This is most likely to be caused by a 180° rotation of all spins on the layers that were previously oppositely canted, as shown in the inset of Fig. 3b. The critical field as a function of temperature is also shown in Fig. 3b. For comparison, we plot the integrated intensity of the (1,1,3/2) magnetic Bragg peak measured with neutron diffraction in Fig. 3c. We find that H_C scales quite closely with the staggered moment $M^{\dagger}$ (which is proportional to the square-root of the Bragg intensity). The mean-field result for La_2CuO_4 gives

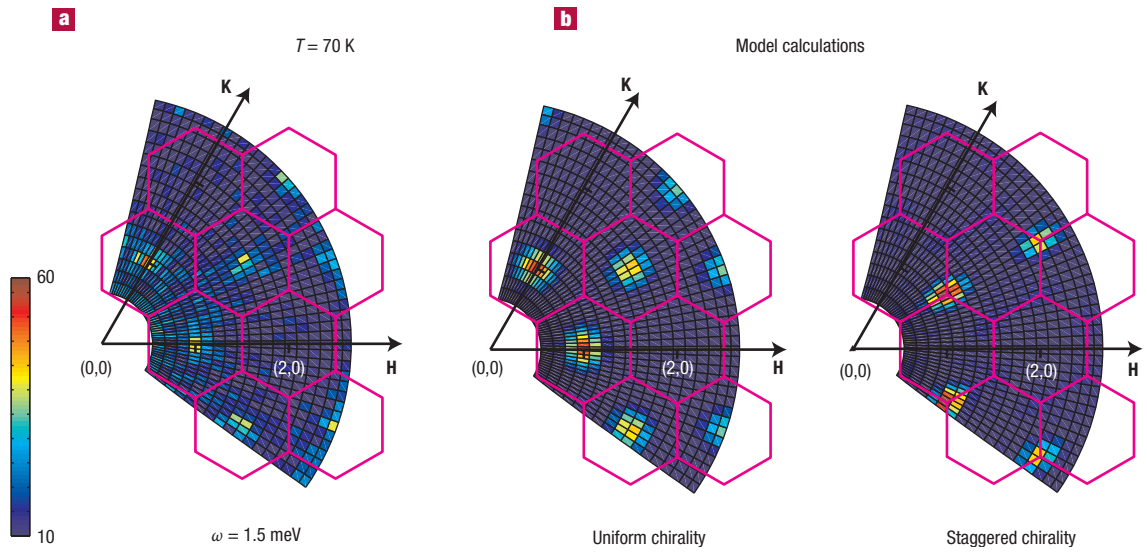

Figure 4 Inelastic neutron scattering data for $KFe_3(OH)_6(SO_4)_2$ measured above T_N, along with structure factor calculations. a, Intensity contour plot of data from inelastic neutron scattering measurements of a single-crystal sample (mass 48 mg). The bright regions are the loci of scattering intensity for the low energy ($\omega = 1.5$ meV) spin fluctuations at $T = 70$ K above T_N. **b**, Model calculations of the intensity as described in the text. The left plot corresponds to short-ranged $q = 0$ correlations with uniform vector chirality, whereas the plot on the right depicts $\sqrt{3} \times \sqrt{3}$ correlations. Both calculations are for the case in which there is no preferred spin direction within the Kagomé plane.

$H_C \propto M^\dagger/\chi^\dagger$, where $\chi^\dagger$ is the 2D staggered susceptibility[22]. In our case, the staggered susceptibility for the Kagomé lattice is expected a have weaker temperature dependence than the square lattice because of the geometrical frustration[23].

Below $T = 49$ K, the critical field becomes larger than 14 T (the maximum field of our magnetometer). Hence, it is difficult to extract the zero-temperature values for H_C and the canted moment. However, an estimate for the canted moment be made by considering the jump in the magnetization near H_C. For the data taken at $T = 50$ K, we obtain a canting angle for the ordered moment of 0.65(6)° with respect to the Kagomé plane for $H \approx H_C$ (this angle will increase on cooling, as the order parameter has not yet reached its low-temperature value). The field-induced transition results from a competition between the interlayer coupling $J_\perp$ and the Zeeman energy; the magnitude of $J_\perp$ may be estimated from the following relation: $H_C(0)\, M_F(0) = 2S^2\, |J_\perp|$, where $H_C(0)$ and $M_F(0)$ are the critical field and ferromagnetic moment per Fe atom, respectively, at $T = 0$. Our results indicate $|J_\perp| = 0.007(6)$ meV where the large error bar comes from the uncertainty in extrapolating H_C and M_F to $T = 0$. We find that the magnitude of $J_\perp$ is several hundred times smaller than the nearest-neighbour J, attesting to the two-dimensionality of the system.

The field-induced spin-canting transition corresponds to a non-trivial change in the spin-texture of the jarosite sample. In particular, the transition yields a net, non-zero value for the scalar chirality, defined on each triangular plaquette as

$$K_S = \mathbf{S}_1 \cdot (\mathbf{S}_2 \times \mathbf{S}_3) \qquad (5)$$

The presence of this type of chirality (in static or fluctuating forms) can have important consequences in strongly correlated electron systems, such as yielding an anomalous Hall effect in metallic materials[10,11]. For $H < H_C$ the net scalar chirality for our jarosite sample is zero because the contributions from neighbouring planes are equal and opposite. However, for $H > H_C$ the spins flip (as depicted in Fig. 3b), and the net scalar chirality becomes non-zero. There are few materials with non-zero scalar chirality in the ordered state, especially on a two-dimensional lattice. In iron jarosite, we have discovered a phase transition in which a net scalar chirality can be 'switched on' by a magnetic field.

NEUTRON SCATTERING AND SPIN FLUCTUATIONS

To probe the microscopic behaviour of the magnetism in the temperature regime above T_N, we made inelastic neutron scattering measurements of the spin fluctuations at $T = 70$ K within the $L = 0$ plane of reciprocal space. For the temperature range $T_N < T < 120$ K, the susceptibilities for $H \,||\, c$ and $H \,||\, ab$ deviate from each other, indicative of the growing influence of spin anisotropy. For the three-dimensionally ordered spin structure below T_N, the stacking arrangement of the planes doubles the magnetic unit cell with respect to the structural unit cell, such that the magnetic Bragg peaks occur at half-odd-integer values of L ($L \neq 0$). However, for temperatures above T_N, the correlations between layers are destroyed, and the 2D spin fluctuations yield 'rods' of scattering in reciprocal space along the L direction. We have verified that all of the signal in Fig. 4a disappears on cooling below T_N, as expected for the transfer of the intensity of the 2D critical scattering into 3D Bragg points lying out of the scattering plane. Therefore, the scans in Fig. 4a pass through the 2D rods of scattering and directly measure the dynamic structure factor of the spin correlations of the single Kagomé planes in iron jarosite. The instantaneous spin correlation length, measured separately in an energy-integrating configuration, is $\xi = 20(2)$ Å at this temperature.

A reciprocal space map of the intensity of the spin fluctuations is shown in Fig. 4a. Outlined in red are the boundaries of the structural Brillouin zones. The strongest scattering occurs at the centres of certain Brillouin zones. The neutron scattering intensity can be calculated by

$$I \propto f(\mathbf{Q})^2 \sum_{\alpha,\beta} \left(\delta_{\alpha,\beta} - \hat{Q}_\alpha \hat{Q}_\beta\right) S^{\alpha,\beta}(\mathbf{Q},\omega) \qquad (6)$$

where α, β refer to x,y,z vector components, $f(\mathbf{Q})$ is the magnetic form factor, and $S(\mathbf{Q},\omega)$ is the space and time Fourier transform of the spin–spin correlation function. The intensity variation reveals a wealth of information about the short-range ordered state in the critical regime just above T_N.

First, the fact that the intensities are centred within the structural Brillouin zones indicates that the fluctuations have the $q = 0$ arrangement. The absence of scattering at the (2,0,0) position is consistent with this spin arrangement. Second, the nearly equivalent intensities at the (1,0,0) and (1,1,0) positions reveal that the spin direction on each sublattice is not fixed. Rather, the two orthogonal spin directions within the Kagomé plane are equally likely. Hence the spin fluctuations have XY symmetry at this temperature (the spin-rotational symmetry within the Kagomé plane is not broken). In contrast, at low temperatures in the 3D ordered state, a preferred spin direction is chosen, and the intensities at (1,0,L) and (1,1,L) differ considerably[7,24].

The observation of short-range $q = 0$ correlations in the 2D fluctuations implies a particular arrangement of the vector chirality. In each region of correlated spins, the vector chirality must be uniform (all positive or all negative for each plaquette). Using equation (6), we calculated the neutron scattering intensity arising from $q = 0$ correlations between coplanar spins assuming only positive chirality. Our model calculations are based on 7-unit-cell clusters of spins, and we have averaged over all spin directions within the Kagomé plane. The results are shown in Fig. 4b, and the agreement with the data is excellent. Also shown in Fig. 4b is a calculation for the intensity if the chirality were staggered as in the $\sqrt{3} \times \sqrt{3}$ arrangement. If such correlated regions exist, the error bars on our data indicate that the fraction must be less than 5%.

Our results shed light on several basic questions regarding the magnetic phase transition in iron jarosite. First, we find that the instantaneous spin correlations above T_N are two-dimensional in nature, and the $q = 0$ arrangement is preferred. Therefore, the selection of $q = 0$ order (as opposed to $\sqrt{3} \times \sqrt{3}$ order which is predicted to be the preferred ground state for the pure Heisenberg model[4,25]) is caused by interactions within a single Kagomé layer and is not controlled by the interplanar interaction[26]. Second, our neutron measurements reveal critical spin fluctuations above T_N that have XY symmetry; hence, the magnetic ordering is not driven by 2D Ising physics[7]. Most interestingly, we find that the spin-rotational symmetry and the vector chiral symmetry are not broken simultaneously at T_N.

The presence of vector chiral order above T_N may be naturally explained in light of the DM interaction. One possibility is that the DM interaction is the dominant source of spin anisotropy in iron jarosite. In this case, the vector chiral order appears concomitantly with the growing spin correlations and does not represent a spontaneously broken symmetry. Another possibility is that the XY anisotropy has an origin (such as symmetric exchange anisotropy[27]) distinct from the DM interaction. Once the spin correlations become coplanar within the Kagomé plane, the vector chirality of a triangular plaquette becomes a discrete symmetry (the chirality vector is either up or down with respect to the c axis). Hence, long-range chiral order is not precluded by the Mermin–Wagner theorem[28]. However, chiral order is easily disrupted on a Kagomé lattice by the proliferation of domain walls (thermally induced defects) which can form with little cost in energy[5,23,29]. Then the presence of a small DM interaction (in particular, the non-zero out-of-plane component D_z) selects a particular chirality for each triangle, and thereby inhibits domain wall formation. It remains possible that the vector chirality represents a spontaneously broken symmetry; however, clarification of this point requires further neutron scattering measurements at higher temperatures.

Our measurements of this ideal Kagomé material reveal new magnetic behaviour related to two types of spin chirality: vector and scalar. The DM interaction is a significant perturbation to the Heisenberg hamiltonian and strongly influences the low-temperature physics. For $T > T_N$, the vector spin chirality is ordered even in the absence of broken spin-rotational symmetry. In the ordered state below T_N, we have discovered a field-induced transition to a state with non-zero scalar chirality. Thus, materials based on jarosites may be promising candidates for studies of the coupling between non-trivial spin textures and the transport of electrons in frustrated systems. For example, carrier-doped compounds would probably show an anomalous Hall effect of topological origin[10], and this might have useful applications in spin-based electronics.

METHODS

The neutron scattering data were taken at the NIST Center for Neutron Research. The integrated intensity of the (1,1,3/2) magnetic Bragg peak (Fig. 3c) was measured using the BT7 spectrometer. The incident neutron energy was fixed at 13.46 meV and the horizontal collimation sequence was open–open–sample–40′–open. The (002) reflection of a pyrolytic graphite crystal was used as an analyser. For the two-axis (energy-integrating) measurement of the instantaneous spin correlation length at $T = 70$ K we used the BT9 spectrometer with the sample aligned in the (HKO) scattering zone. The incident neutron energy was 35 meV, with a collimation sequence of 40′–24′–sample–20′. In both measurements, a pyrolytic graphite filter was placed in the incident beam to remove higher-order neutrons. The inelastic neutron scattering data shown in Fig. 4 were taken using the SPINS NG5 triple-axis spectrometer. The final neutron energy was fixed at 5 meV and the horizontal collimation sequence was guide–80′–sample–40′(radial)–open. A liquid-nitrogen-cooled beryllium filter was placed in the scattered beam to remove higher-order neutrons.

Received 12 November 2004; accepted 08 February 2005; published 27 March 2005.

References

1. Ramirez, A. P. in *Handbook on Magnetic Materials* Vol. 13 (ed. Busch, K. J. H) 423–520 (Elsevier Science, Amsterdam, 2001).
2. Bramwell, S. T. & Gingras, M. J. P. Spin ice state in frustrated magnetic pyrochlore materials. *Science* **294**, 1495–1501 (2001).
3. Harris, A. B., Kallin, C. & Berlinsky, A. J. Possible Néel orderings of the Kagomé antiferromagnet. *Phys. Rev. B* **45**, 2899–2919 (1992).
4. Sachdev, S. Kagomé and triangular-lattice Heisenberg antiferromagnets: ordering from quantum fluctuations and quantum-disordered ground states with unconfined bosonic spinons. *Phys. Rev. B* **45**, 12377–12396 (1992).
5. Chalker, J. T., Holdsworth, P. C. W. & Shender, E. F. Hidden order in a frustrated system: properties of the Heisenberg Kagomé antiferromagnet. *Phys. Rev. Lett.* **68**, 855–858 (1992).
6. Ritchey, I., Chandra, P. & Coleman, P. Spin folding in the two-dimensional Heisenberg Kagomé antiferromagnet. *Phys. Rev. B* **47**, 15342–15345 (1993).
7. Inami, T., Nishiyama, M., Maegawa, S. & Oka, Y. Magnetic structure of the Kagomé lattice antiferromagnet potassium jarosite $KFe_3(OH)_6(SO_4)_2$. *Phys. Rev. B* **61**, 12181–12186 (2000).
8. Wills, A. S. Long-range ordering and representational analysis of the jarosites. *Phys. Rev. B* **63**, 064430 (2001).
9. Wen, X. G., Wilczek, F. & Zee, A. Chiral spin states and superconductivity. *Phys. Rev. B* **39**, 11413–11423 (1989).
10. Ohgushi, K., Murakami, S. & Nagaosa, N. Spin anisotropy and quantum Hall effect in the Kagomé lattice: chiral spin state based on a ferromagnet. *Phys. Rev. B* **62**, R6065–R6068 (2000).
11. Taguchi, Y., Oohara, Y., Yoshizawa, H., Nagaosa, N. & Tokura, Y. Spin chirality, Berry phase, and anomalous Hall effect in a frustrated ferromagnet. *Science* **291**, 2573–2576 (2001).
12. Wills, A. S., Harrison, A., Ritter, C. & Smith, R. I. Magnetic properties of pure and diamagnetically doped jarosites: model Kagome antiferromagnets with variable coverage of the magnetic lattice. *Phys. Rev. B* **61**, 6156–6169 (2000).
13. Nocera, D. G., Bartlett, B. M., Grohol, D., Papoutsakis, D. & Shores, M. P. Spin frustration in 2D Kagomé lattices: a problem for inorganic synthetic chemistry. *Chem. Eur. J.* **10**, 3850–3859 (2004).
14. Kawamura, H. in *Proc. Workshop on Low-Dimensional Quantum Antiferromagnets* (Fukuoka, November 2001); cond-mat/0202109.
15. Calabrese, P. & Parruccini, P. Critical behavior of two-dimensional frustrated spin models with noncollinear order. *Phys. Rev. B* **64**, 184408 (2001).
16. Mason, T. E., Gaulin, B. D. & Collins, M. F. Neutron scattering measurements of critical exponents in $CsMnBr_3$: a $Z_2 \times S_1$ antiferromagnet. *Phys. Rev. B* **39**, 586–590 (1989).
17. Plakhty, V. P. *et al.* Chiral criticality in helimagnet Ho studied by polarized neutron scattering. *Phys. Rev. B* **64**, 100402 (2001).
18. Grohol, D., Nocera, D. G. & Papoutsakis, D. Magnetism of pure iron jarosite. *Phys. Rev. B* **67**, 064401 (2003).
19. Elhajal, M., Canals, B. & Lacroix, C. Symmetry breaking due to Dzyaloshinsky–Moriya interactions in the Kagomé lattice. *Phys. Rev. B* **66**, 014422 (2002).
20. Moriya, T. Anisotropic superexchange interaction and weak ferromagnetism. *Phys. Rev.* **120**, 91–98 (1960).
21. Wells, B. O. *et al.* Intercalation and staging behavior in super-oxygenated La_2CuO_{4+d}. *Z. Phys. B* **100**, 535–545 (1996).
22. Thio, T. *et al.* Antisymmetric exchange and its influence on the magnetic structure and conductivity of La_2CuO_4. *Phys. Rev. B* **38**, 905–908 (1988).

23. Reimers, J. N. & Berlinsky, A. J. Order by disorder in the classical Heisenberg Kagomé antiferromagnet. *Phys. Rev. B* **48**, 9539–9554 (1993).
24. Nishiyama, M., Maegawa, S., Inami, T., & Oka, Y. Magnetic ordering and spin dynamics in potassium jarosite: a Heisenberg Kagomé lattice antiferromagnet. *Phys. Rev. B* **67**, 224435 (2003).
25. Chubukov, A. Order from disorder in a Kagomé antiferromagnet. *Phys. Rev. Lett.* **69**, 832–835 (1992).
26. Lee, S. H. *et al.* Less than 50% sublattice polarization in an insulating S=3/2 Kagomé antiferromagnet at $T \sim 0$. *Phys. Rev. B* **56**, 8091–8097 (1997).
27. Yildirim, T., Harris, A. B., Aharony, A. & Entin-Wohlman, O. Anisotropic spin Hamiltonian due to spin-orbit and coulomb exchange interactions. *Phys. Rev. B* **52**, 10239–10267 (1995).
28. Mermin, N. & Wagner, H. Absence of ferromagnetism or antiferromagnetism in one- or two-dimensional isotropic Heisenberg models. *Phys. Rev. Lett.* **22**, 1133–1136 (1966).
29. von Delft, J. & Henley, C. L. Spin tunneling in the Kagomé antiferromagnet. *Phys. Rev. B* **48**, 965–984 (1993).

Acknowledgements

We thank A. Clearfield for providing the large hydrothermal vessels used in the crystal growth. We thank Y.-B. Kim, T. Senthil and T. Yildirim for useful discussions. This work was supported in part by the MRSEC Program of the National Science Foundation under award number DMR 02-13282 and also by NSF award DMR-0239377.
Correspondence and requests for materials should be addressed to Y.S.L. or D.G.N.
Supplementary Information accompanies the paper on www.nature.com/naturematerials.

Competing financial interests

The authors declare that they have no competing financial interests.